Indian Journal of Heterocyclic Chemistry
Vol. 33 - Number 04 (Oct-Dec 2023) 499-507
https://connectjournals.com/01951.2023.33.499
https://doi.org/10.59467/IJHC.2023.33.499

ISSN (Print) : 0971-1627
ISSN (Online) : 2456-4311

Synthesis of Some *N*-(1*H*-Benzo[*d*]imidazol-2-yl)-2-(4-Arylpiperazin-1-yl) acetamides as Anticancer Agents

Haythem Saadeh[1], Raneem Kaddoura[2], Ismail El-Haty[3], Mohammad Khasawneh[2], Abdelouahid Samadi[2], Abdelhabib Semlali[4] and Nael Abutaha[5]*

[1]Department of Chemistry, School of Science, The University of Jordan, Amman 11942, Jordan
[2]Department of Chemistry, College of Science, United Arab Emirates University, P. O. Box 15551, Al Ain, United Arab Emirates
[3]Department of Nutrition and Dietetics, School of Health Sciences, Istanbul Gelisim University, Istanbul, Turkey
[4]Groupe de Rechercheen Écologie Buccale, Faculté de Médecine Dentaire, Université Laval, Québec, Canada
[5]Department of Zoology, College of Science, King Saud University, Riyadh, Saudi Arabia

ABSTRACT A series of eight *N*-(1*H*-benzo[*d*]imidazol-2-yl)-2-(4-arylpiperazin-1-yl)acetamides was synthesized as potential anticancer agents. Reacting 2-aminobenzimidazole (**1)** with 2-chloroacetyl chloride in the presence of the base gave N-(1*H*-benzo[d]imidazol-2-yl)-2-chloroacetamide (**2)** which then reacted with substituted piperazines **3a-h** to give the targeted compounds **4a-h**. The cytotoxic activity of lung (A549) and liver (HepG2) human cancer cells was assessed using the MTT assay. The results demonstrated that IC_{50} values of **4b**, **4c**, **4g**, and **4h** were 4.8 µM, 13.3 µM, 5.1µM, and 11.5 µM on HepG2 cells, respectively. Similarly, the IC_{50} values of **4b**, **4c**, **4g**, and **4h** were 56.9 µM, 46.6 µM, 53.2 µM, and 59.4 µM on A549 cells after 48 h treatment, respectively. The compounds showed higher anticancer activity against HepG2 cells than A549 cells. Compound **4b** and **4g** mediated cytotoxicity in HepG2 cells by inducing apoptotic cell death, as revealed by fluorescence microscopy. An *in silico* study was carried out to study the interactions with the active binding site of different receptors. Vascular endothelial growth factor receptor 2 crystal structures (PDB ID; 4ASD) indicated a strong binding mode of **4g** compound (ΔG=−10.28 kcal/mol), corresponding with their cytotoxic activities.

KEYWORDS Anticancer activity, Apoptosis, Benzimidazole, Piperazines.

How to cite this article: Saadeh, H., Kaddoura, R., El-Haty, I., Khasawneh, M., Samadi, A., Semlali, A. and Abutaha, N. Synthesis of Some *N*-(1*H*-Benzo[*d*]imidazol-2-yl)-2-(4-arylpiperazin-1-yl)acetamides as Anticancer Agents, *Indian J. Heterocycl. Chem.*, **2023**, *33*, 499–507. (https://doi.org/10.59467/IJHC.2023.33.499)

INTRODUCTION

The nitrogen-containing heterocycles play an important role in mankind. Benzimidazole is a heterocyclic system that attracted the attention of researchers worldwide due to its wide range of therapeutic activities. The activity of benzimidazole derivatives is continuously reviewed.[1-5] Some of the pharmacological activities which have been reported include anticancer, antiviral, antibacterial, anthelmintic, anti-inflammatory, antiparasitic, antifungal, analgesic, antiulcer anticonvulsant, anticoagulant, proton pump inhibition, and antihypertensive.

Cancer is one of the leading causes of death worldwide due to its complexity and high mortality rate, accounting for nearly 10 million deaths in 2020.[6] Hepatocellular carcinoma constitutes 75% of diagnosed liver cancer. In 2021, liver cancer caused 30,230 deaths. The 5-year survival rate for liver cancer is 20%, despite the improvement in surgery and the development of tumoricidal drugs.[7] The need to discover new cancer agents with high selectivity and low side effects is immediate and a serious challenge too. Among the recently discovered anticancer agents,[8] various benzimidazole derivatives possess potent anticancer properties,[9,10] and some have found their way into the drug market such as nocodazole and veliparib.

*Corresponding author: Email: nabutaha@ksu.edu.sa

Published & Hosted by :
Journal Homepage :
www.connectjournals.com/ijhc
www.connectjournals.com

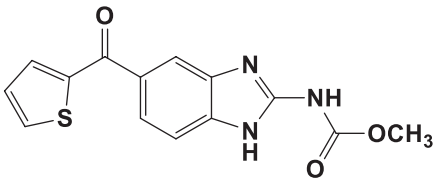

Nocodazole

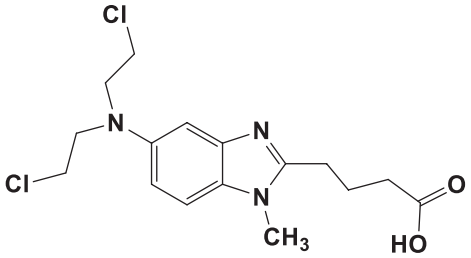

Veliparib

Considering the significance of the benzimidazoles activity profile and as an extension of our research on synthesizing new anticancer agents,[11] we describe herein the synthesis of a number of new benzimidazole-substituted piperazine derivatives and assess their anticancer potential against liver and lung cancer cells.

RESULTS AND DISCUSSION

Chemistry

Five new benzimidazole-piperazine derivatives (**4b**,**4d**, **4e**, **4g**, and **4h**) and three previously reported (**4a**, **4c**, and **4f**)[12] were synthesized according to [**Scheme 1**]. The first step of synthesis involved the reaction of 2-aminobenzimidazole (**1**) with chloroacetyl chloride in the presence of sodium carbonate to give N-(1*H*-benzo[d]imidazole-2-yl)-2-chloroacetamide (**2**). The compound **2** was subjected to the reaction with substituted piperazines **3a-h** in the presence of excess Et_3N to afford the target products **4a-h**. All compounds were purified and characterized by ^{13}C-NMR and ^{1}H-NMR and confirmed by high-resolution mass (HRMS). The ^{1}H NMR displayed the presence of benzimidazole protons at 6.70–7.10 ppm and the piperazine protons at about 2.70 and 3.30 ppm. The ^{13}C NMR spectra of the compounds are consistent with the proposed compounds. IR spectra showed the absorption bands corresponding to amide N-H and C═O groups where their stretching vibrations appeared at around 3350 and 1690 cm^{-1}, respectively. This spectral data is in agreement with the proposed structures. The HRMS displayed the correct molecular ion peaks for each derivative and were very close to the calculated values. The variation in the suggested compounds [**Scheme 1**] is apparent from the diverse substitutions on the phenyl ring including deactivating and activating groups. These different substitutions could help finding relationships between the chemical structure and biological activity of studied derivatives.

In silico molecular docking

The compound, **4g**, was selected from the series to analyze its binding mode against the active pocket because it showed the highest binding affinity compared to other compounds tested. Computational studies were carried out to assess the binding mode action of **4g** against the vascular endothelial growth factor receptor 2 (VEGFR-2) target protein (PDB

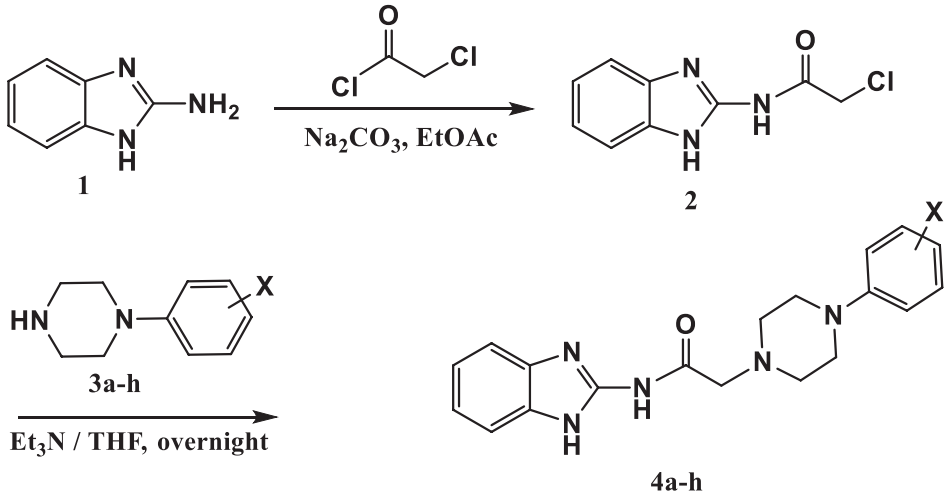

a	b	c	d	e	f	g	h
H	4-CH_3	4-OCH_3	4-F	3-F	2-F	4-CF_3	4-Cl

Scheme 1: Synthesis of benzimidazole-piperazine derivatives 4a-h

ID; 4ASD). The docking studies showed that the amide moiety interacted with the receptor through five hydrogen bonds with Asp1046, Glu885, and Lys868 protein residues. Moreover, the nitrogen of the piperazine ring formed a hydrogen bond with Asp104. Furthermore, the benzene ring and CF_3 moieties formed five hydrophobic interactions with Leu1035, Leu1033, Ala866, Leu840, Val848, and Leu889. In addition, a salt bridge with residue Glu885 and a halogen bond with Cys919 were also formed. Salt bridge, halogen bond, and hydrogen bond interactions play a key role in protein-ligand stability [**Table 1** and **Figure 1**].[13-15]

Biology

Cell viability

The MTT assay was carried out against HepG2 and A549 cancer cell lines to investigate the cytotoxic potential of benzimidazole-piperazine derivatives. It was observed that only **4b**, **4c**, **4g,** and **4h** inhibited the growth of these cancer cells dose-dependently. Results demonstrated that IC_{50} values of **4b**, **4c**, **4g,** and **4h** were 4.8 µM, 13.3 µM, 5.1µM, and 11.5 µM on HepG2 cells, respectively. Similarly, the IC_{50} values of **4b**, **4c**, **4g,** and **4h** were 56.9 µM, 46.6 µM, 53.2 µM, and 59.4 µM on A549 cells after 48 h treatment, respectively [**Figure 2**]. Results revealed that liver cancer cells (HepG2) were more sensitive to all compounds tested than lung cancer cells (A549). The most promising compounds were **4b** and **4g**. Based on the obtained results, we proceeded to further investigate compounds 4b and 4g.

Light microscopy

To investigate the cytotoxic activities of **4b** and **4g**, the morphological changes in HepG2 cells were assessed by light microscopy. Light microscopic observations of HepG2 cells post-treatment with **4b** and **4g** for 48 h showed lower cell confluency than control cells. Furthermore, treatment of HepG2 cells with **4b** and **4g** resulted in floating cells and decreased adherence [**Figure 3b** and **c**]. Control (untreated) cells were confluent and attached to the culture plates [**Figure 3a**].

Table 1: Docked score (GlideScore) and residues of different target proteins forming hydrogen bonds and hydrophobic interactions

S. No.	Compounds	GlideScore (kcal/mol)	Hydrogen bonds	Hydrophobic interactions
1.	**4FA6**			
	4b	−9.3	GLN291, ARG690	ARG294, LYS 298, PHE694, ARG849
	4g	−9.7	GLN291, ARG690, GLU856	ARG294, LYS298, PHE694, ARG849
2.	**5EKN**			
	4b	−9.1	GLU72, ASP168	VAL39, ILE85, PHE109, LEU167, ASP168
	4g	−9.5	GLU72, ASP168	VAL39, LEU76, MET79, VAL84, LEU167, PHE169
3.	**1M17**			
	4b	−7.9	LYS721, ASP813	PHE699, LYS721, GLU722, LEU723, ILE735
	4g	−8.1	ARG817, ASN818, ASP831	PHE699, VAL702, LYS721, ASP831, LEU834
4.	**6OQO**			
	4b	−8.5	TYR24, LYS147	VAL181, ALA162, LEU152, PHE98, VAL77, ALA41, VAL27
	4g	−9.7	TYR24, LYS147	VAL181, ALA162, LEU152, PHE98, VAL77, ALA41, VAL27,
5.	**4ASD**			
	4b	−9.2	LYS686, GLU858, ASP1046	LEU840, VAL848, ALA866, LEU889, ILE892, PHE918, LEU1035, ASP1046, PHE1047
	4g	−10.8	LYS868, GLU885, ASP1046	VAL848, ALA866, LYS868, VAL899, VAL916, LEU1035, ASP1046, PHE1047
6.	**4UMT**			
	4b	−10.3	ASP170	ILE17, VAL25, ALA38, LEU61, LEU139, ASP150
	4g	−10.6	GLU57, ALA129, ARG131	LEU61, LEU64, MET84, TYR128, HIS130, ILE149, ASP150, PHE151
7.	**4NUD**			
	4b	−8.2	ASN140	TRP81, PRO82, PHE82, VAL87, LEU92, MET132, CYS136
	4g	−8.3	ASN140, ASP144	PHE83, VAL87, LEU94, TYR97, ASN140, ILE146
8.	**1XO2**			
	4b	−8.9	ARG30, GLU31, HIS67, VAL150	LEU34, VAL77, ALA149, PRO195, ILE198
	4g	−9.7	LEU40, ALA191	LEU34, LYS36, SER39, PRO74, ARG82, LEU185, LEU192

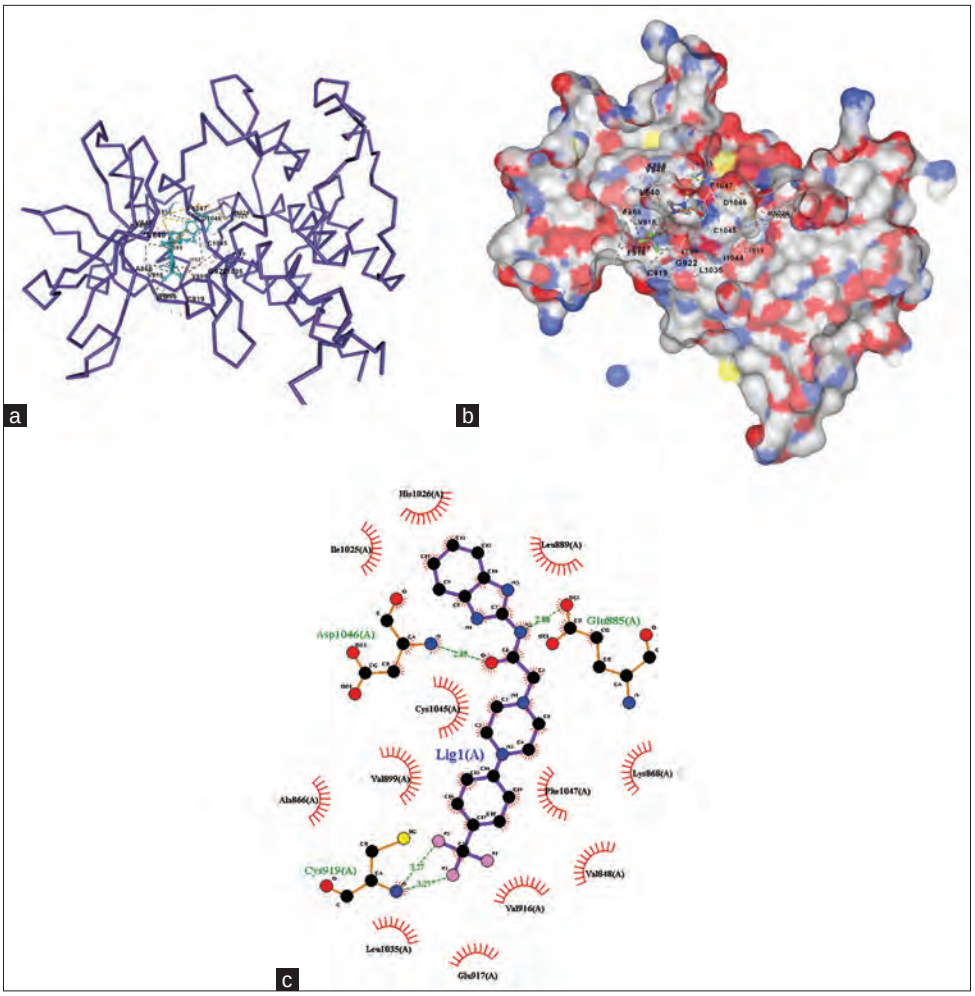

Figure 1: Molecular docking of 4g with VEGFR2 4ASD: (a) 4ASD protein structure domains and active site (represented in color) and best dock pose of the compounds, (b) The surface structure of 4ASD binding with 4g at the active site, (c) 2D structure of 4g interacting with 4ASD active site residues

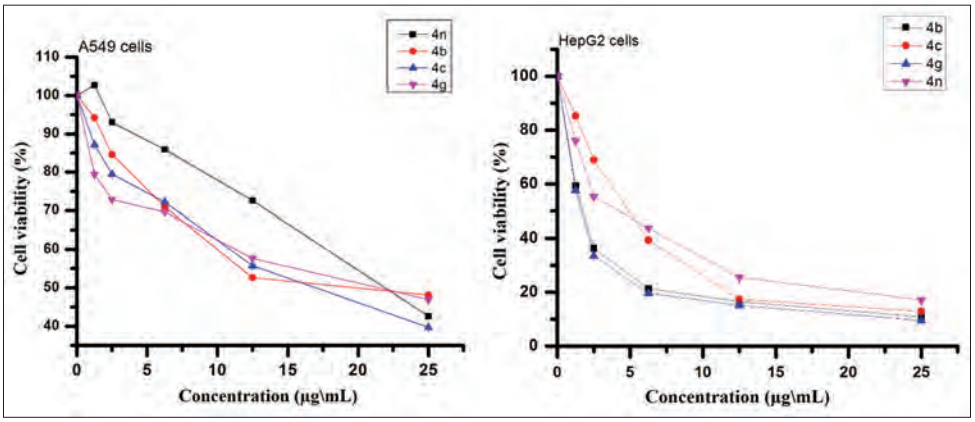

Figure 2: Cytotoxicity of 4b, 4c, 4g, and 4h in HepG2 and A549 human cancer cells using MTT assay. Results were normalized using cells treated with 1% DMSO in a complete growth medium representing 100% survival

4',6-Diamidino-2-phenylindole (DAPI) staining

DAPI staining was employed to assess chromatin condensation or nuclear damage. Therefore, this method was carried out to assess the apoptosis induction of **4b** and **4g** in HepG2 cells, respectively. From **Figure 3**, the nuclei and chromatin of control cells displayed an intact nuclear structure [**Figure 3d**]. In contrast, cells treated with **4b** and **4g** displayed condensed or fragmented nuclei [**Figure 3e** and **f**].

Acridine orange/ethidium bromide (AO/EB) staining

AO/EB staining helps to discriminate between necrotic, apoptotic, and live cells. AO can permeate the membrane

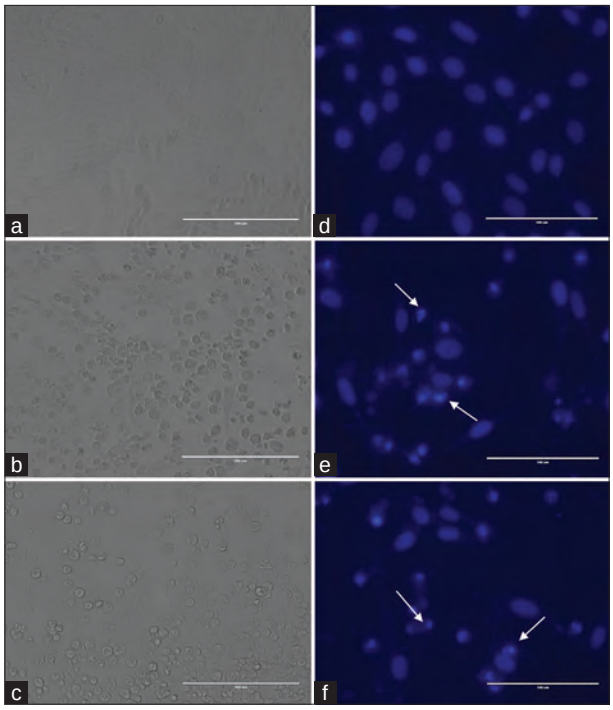

Figure 3: Cell morphology of control (a) and HepG2 cells treated with compounds 4b (b) and 4g (c). (d) Apoptotic nuclear cell morphology using DAPI staining: It displays the effect of 4b (e) and 4g (f) treatments on liver cancer cells (HepG2) post 48 h incubation. Figure D represents the control

of live cells (intact) and stain the nuclei green, whereas EB stains the cell nuclei that have lost their membrane integrity and stain the nuclei red. It can be observed that the cells in the control group appeared green in color and showed normal morphology [**Figure 4**]. In contrast, in the group treated with **4b** and **4g**, the number of cells was decreased, and fragmented green nuclei (apoptosis) and red-fluorescent cells (necrosis) were observed [**Figure 4**]. HepG2 cells treated with **4b** and **4g** exhibited morphological alternation such as chromatin condensation, shrinkage, and membrane blebbing. Therefore, it was confirmed that **4b** and **4g** caused liver cell necrosis and apoptosis when cells were incubated with **4b** and **4g**.

Necrosis, autophagy, and apoptosis are processes that can cause cell death. Most anticancer drugs act mechanistically through apoptosis induction.[16] Apoptosis is an essential mechanism that controls the cell numbers by removing the unwanted cells. When anticancer chemotherapeutic agents induce apoptosis, several biochemical and morphological changes, such as membrane blebbing, chromosomal condensation, release of cytochrome c, and DNA fragmentation occur.[17,18] DAPI and AO/EB Annexin results confirmed that **4g** and **4b** induced apoptosis in HepG2 cancer cells.

VEGFR-2 has been approved as a target for several inhibitors to treat cancer.[19,20] Studying the binding mode of VEGFR-2 inhibitors revealed that they have four pharmacophoric sites that facilitate their interactions with the active binding site.[21,22] The first feature includes the presence of one H-bond acceptor to interact with Cys919 in the hinge region.[20,23] Another feature is a spacer group that provides the inhibitor with the proper length,[24,25] making the DFG motif and pharmacophore (such as urea or amide) close enough to bind with Asp1044 and Glu883.[24,26] The last site is the terminal hydrophobic moiety that resides in the allosteric hydrophobic binding pocket.[27]

This report shows that **4g** and **4b** are novel and promising anticancer therapeutic agent candidates. We found that **4g** and **4b** have potential therapeutic applications in cancer and may be attributed to apoptosis and necrosis of liver cancer cells. Future optimization based on the biological and docking studies will be carried out.

EXPERIMENTAL SECTION

All chemicals and reagents were purchased from ACROS ORGANICS (Sigma Aldrich, USA) and used without further purification. Column chromatography was conducted on silica Gel 60 (230 mesh) and thin-layer chromatography analyses were performed on silica F254 with detection using UV light. Melting points were determined in an open capillary tube using Sanyo Gallenkamp MPD 350-BM 3.5 (UK) and were uncorrected. FT-IR, ^{1}H NMR, and ^{13}C NMR spectra were recorded using Thermo Nicolet Nexus 470 (USA) and a Varian-400 MHz (USA) instruments, respectively, at 25°C in $CDCl_3$ or DMSO d6 at 400 MHz, with solvent peaks [$CDCl_3$: 7.26 (D) and 77.2 (C) ppm and DMSO d6: 2.50 (D) and 39.7 (C) ppm] as internal references. HRMS spectra were obtained $[M-H]^-$ using electrospray ion trap (ESI) negative ion mode technique with collision-induced dissociation on a Bruker APEX-4 (7-Tesla) instrument.

Synthesis of *N*-(1*H*-benzo[d]imidazol-2-yl)-2-chloroacetamide (2)

A solution of 2-aminobenzimidazole **1 (**4.0g, 30 mmol) and anhydrous sodium carbonate (3.81g, 36 mmol) in dry ethyl acetate (200 mL) was stirred at 0°C and added a solution of 2-chloroacetyl chloride (5.6 mL, 70 mmol) in 10 mL of ethyl acetate dropwise. The mixture was stirred for 30 min, and the reaction progress was monitored by TLC. After filtration of the slurry, the filtrate was evaporated using a rotary evaporator to yield a solid residue. The obtained solid was recrystallized from ethyl acetate, resulting in the formation of an off-white solid (3.7 g, 48.5%); mp: 196–199°C (lit. 198–201°C);[28] FT-IR (KBr, ν_{max}/cm^{-1}): 3328 (N-H), 1692 (C=O), ^{1}H NMR (400 MHz, DMSO-d_6) (ppm): 4.65 (s, 2H); 7.08 (m, 2H); 7.41 (m, 2H); 12.05 (s, 2H); ^{13}C NMR (400 MHz, DMSO-d_6) (ppm): 42.3; 114.4; 121.9; 135.8; 147.1; 167.5.

General procedure for the synthesis of compounds 4a-h

A solution of *N*-(1H-benzo[d]imidazol-2- yl)-2-chloroacetamide **(2)** (210 mg, 1.0 mmol) and excess triethylamine (280 µL, 2.0 mmol) in dry THF (20 mL) was treated with 1 mmol of substituted piperazines (3a-h). The mixture was stirred overnight at room temperature. The obtained crude product was washed with water followed by

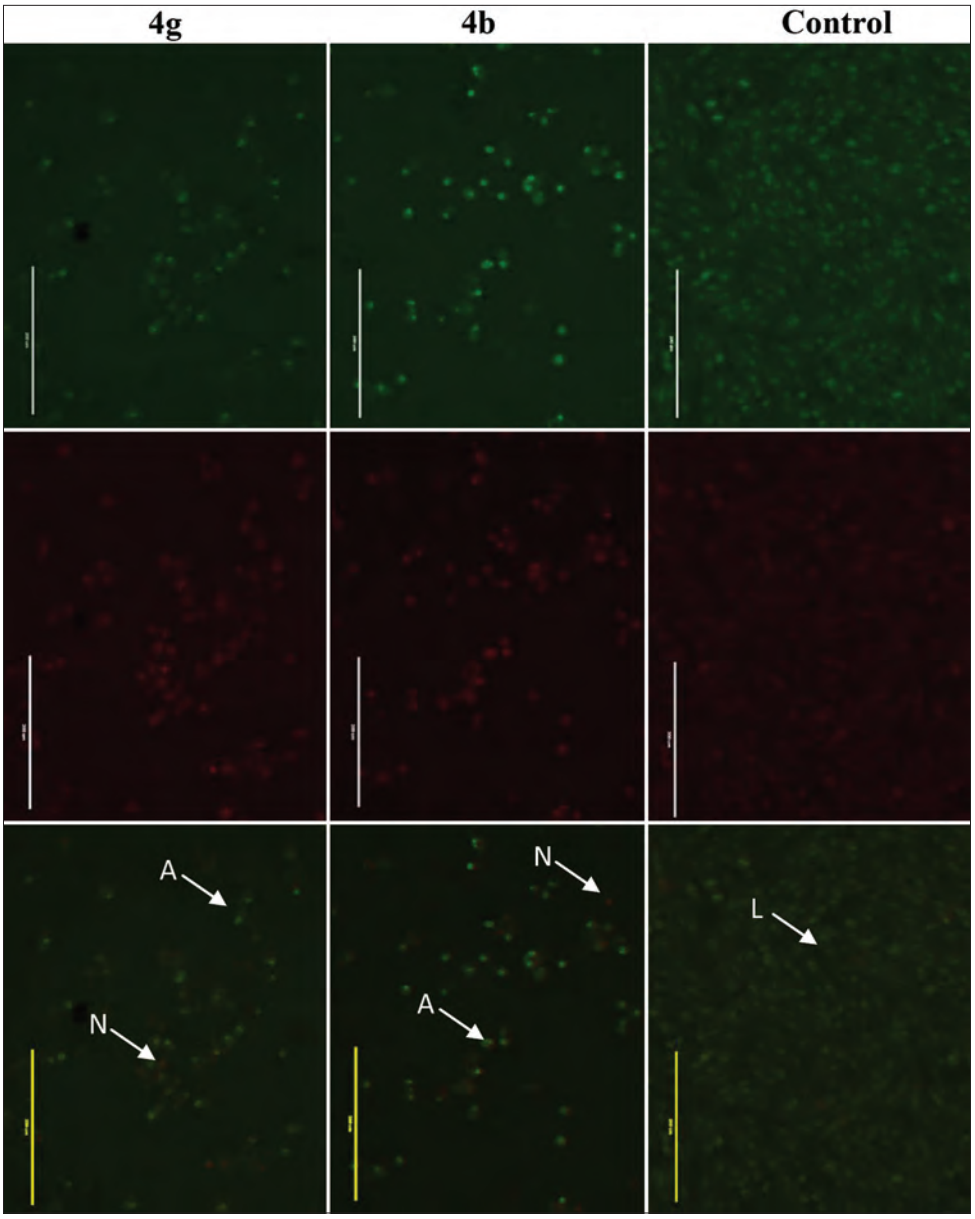

Figure 4: Staining of HepG2 cells with AO/EB post-incubation with 4b and 4g. Cells were incubated with 4b and 4g at $2IC_{50}$ and compared with control (1% DMSO). N: Necrotic cells, A: Apoptotic cells, E: Early apoptotic cells, L: Living cells

ethyl acetate. The solid was recrystallized from ethanol and dichloromethane to afford the pure product (**4a-h**).

***N*-(1*H*-Benzo[d]imidazol-2-yl)-2-(4-phenylpiperazin-1-yl)acetamide (4a).**[13] Off-white solid; (0.130 g, 38.8%); mp: 256–258°C; FT-IR (KBr, ν_{max}/cm^{-1}): 3345 (N-H), 1690 (C=O), ^{1}H NMR (400 MHz, DMSO-d_6) (ppm): 2.80 (t, *J*=4.0 Hz, 4H); 3.26 (t, *J*=4.0 Hz, 4H); 3.31 (s, 2H); 6.87 (m, 3H); 7.29 (m, 4H); 7.29 (m,2H);10.82 (s, H). ^{13}C NMR (400 MHz, DMSO-d_6) (ppm): 48.67; 52.89; 60.89; 111.88; 115.87; 119.25; 121.47; 129.35; 133.55; 146.49; 151.40; 169.88. HRMS (ESI): m/z calcd for $C_{19}H_{22}N_5O$ [M+H] 336.18244, found 336.18283.

***N*-(1*H*-Benzo[d]imidazol-2-yl)-2-(4-(p-tolyl) piperazin-1-yl)acetamide (4b).** White solid. (0.138 g, 39.4%); mp: 236–237°C; FT-IR (KBr, ν_{max}/cm^{-1}): 3361 (N-H), 1688 (C=O), ^{1}H NMR (400 MHz, DMSO-d_6) (ppm): 2.16 (s, 3H); 2.68 (t, *J*=4.0 Hz, 4H); 3.09 (t, *J*=4.0 Hz, 4H); 3.31 (s, 2H); 6.81 (d, *J*=8.0, 2H); 6.99 (d, *J*=8.0 Hz, 2H); 7.05 (m, 2H); 7.40 (s, 2H); 11.15 (s, 1H); 12.05 (s, 1H). ^{13}C-NMR (400 MHz, DMSO-d_6) (ppm): 20.47; 49.16; 52.94; 60.92; 111.96; 116.15; 121.59; 128.06; 128.79; 140.91; 146.48; 149.34; 169.88. HRMS (ESI): m/z calcd for $C_{20}H_{24}N_5O$ [M+H] 350.19809, found 350.19834.

***N*-(1*H*-Benzo[d]imidazol-2-yl)-2-(4-(4-methoxyphenyl)piperazin-1-yl)acetamide (4c).**[13] Off-white solid; (0.168 g, 42.0%); mp: 235–237°C; FT-IR (KBr, ν_{max}/cm^{-1}): 3348 (N-H), 1685(C=O), ^{1}H NMR (400 MHz, DMSO-d_6) (ppm): 2.68 (t, *J*=4.0 Hz, 4H); 3.03 (t, *J*=4.0 Hz, 4H); 3.31 (s, 2H); 3.65 (s, 3H); 6.78 (d, *J*=8.0 Hz, 2H); 6.86 (d, *J*=8.0 Hz, 2H); 7.05 (m, 2H); 7.41 (s, 2H); 11.15 (s, 1H); 12.05 (s, 1H). ^{13}C NMR (400 MHz, DMSO-d_6) (ppm): 50.07; 53.04; 55.61; 60.92; 112.12; 114.67; 117.86; 121.50;

133.14; 145.79; 146.48; 153.34; 169.88. Anal. Calcd for $C_{20}H_{23}N_5O_2$: C, 65.73; H, 6.34; N, 19.16. Found: C, 64.61; H, 6.34; N, 18.92. HRMS (ESI): m/z calcd for $C_{20}H_{24}N_5O_2$ [M+H] 366.19300, found 366.19355.

***N*-(1*H*-Benzo[d]imidazol-2-yl)-2-(4-(4-fluorophenyl) piperazin-1-yl)acetamide (4d).** White solid; (0.103 g, 29.1%); mp: 227–230°C; FT-IR (KBr, ν_{max}/cm^{-1}): 3327 (N-H), 1697 (C=O), ^{1}H NMR (400 MHz, DMSO-d_6) (ppm): 2.69 (t, *J*=4.0 Hz, 4H); 3.10 (t, *J*=4.0 Hz, 4H); 3.32 (s, 2H); 6.90–7.06 (m, 6H); 7.41 (s, 2H); 11.16 (s, 1H); 12.06 (s, 1H). ^{13}C-NMR (400 MHz, DMSO-d_6) (ppm): 49.45; 52.88; 60.85; 111.96; 115.68 (d); 117.60 (d); 121.45; 140.84; 146.48; 148.33; 156.43 (d); 169.85. HRMS (ESI): m/z calcd for $C_{19}H_{21}FN_5O$ [M+H] 354.17301, found 354.17336.

***N*-(1*H*-Benzo[d]imidazol-2-yl)-2-(4-(3-fluorophenyl) piperazin-1-yl)acetamide (4e)**. Off-white solid; (0.110 g, 31.2%); mp: 213–215°C; FT-IR (KBr, ν_{max}/cm^{-1}): 3365 (N-H), 1689 (C=O), ^{1}H NMR (400 MHz, DMSO-d_6) (ppm): 2.67 (t, *J*=4.0 Hz, 4H); 3.20 (t, *J*=4.0 Hz, 4H); 3.32 (s, 2H); 6.68–7.07 (m, 6H); 7.42 (s, 2H); 11.29 (s, 1H); 11.87 (s, 1H). ^{13}C NMR (400 MHz, DMSO-d_6) (ppm): 48.13; 52.64; 60.81; 102.21 (d); 105.05 (d); 111.30; 111.98; 121.48; 130.73 (d); 140.48; 146.50; 153.15 (d); 163.71 (d); 169.86. HRMS (ESI): m/z calcd for $C_{19}H_{21}FN_5O$ [M+H] 354.17301, found 354.17320.

***N*-(1*H*-Benzo[d]imidazol-2-yl)-2-(4-(2-fluorophenyl) piperazin-1-yl)acetamide (4f).**[13] White solid; (0.130 g, 36.5%); mp: 227–228°C; FT-IR (KBr, ν_{max}/cm^{-1}): 3363 (N-H), 1690 (C=O), ^{1}H NMR (400 MHz, DMSO-d_6) (ppm): 2.72 (t, *J*=4.0 Hz, 4H); 3.04 (t, *J*=4.0 Hz, 4H); 3.33 (s, 2H); 6.91–7.11 (m, 6H); 7.41 (s, 2H); 11.15 (s, 1H); 12.05 (s, 1H). ^{13}C NMR (400 MHz, DMSO-d_6) (ppm): 50.52; 52.95; 60.88; 111.97; 116.34 (d); 119.71 (d); 121.51; 122.75 (d); 125.25 (d); 140.26 (d); 140.78; 146.50; 155.38 (d,); 169.88. HRMS (ESI): m/z calcd for $C_{19}H_{21}FN_5O$ [M+H] 354.17301, found 354.17347.

***N*-(1*H*-Benzo[d]imidazol-2-yl)-2-(4-(4-(trifluoromethyl)phenyl)piperazin-1-yl)acetamide (4g).** Off-white solid; (0.162 g 40.2%); mp: 240–242°C; FT-IR (KBr, ν_{max}/cm^{-1}): 3367 (N-H), 1686 (C=O), ^{1}H NMR (400 MHz, DMSO-d_6) (ppm): 2.69 (t, *J*=4.0 Hz, 4H); 3.30 (t, *J*=4.0 Hz, 4H); 3.34 (s, 2H); 7.01–7.08 (m, 4H); 7.41 (s, 2H); 7.46 (d, *J*=12.0 Hz, 2H); 11.22 (s, 1H); 12.05 (s, 1H). ^{13}C NMR (400 MHz, DMSO-d_6) (ppm): 47.45; 52.50; 60.76; 112.03; 114.64; 118.22 (m); 121.48; 124.08; 126.59 (m); 133.13 (C8, C9); 146.51 (C2); 153.61 (C5''); 169.88 (C2'). HRMS (ESI): m/z calcd for $C_{20}H_{21}F_3N_5O$ [M+H] 404.16982, found 404.17055.

***N*-(1*H*-Benzo[d]imidazol-2-yl)-2-(4-(4-chlorophenyl) piperazin-1-yl)acetamide (4h).** White solid; (0.138 g, 37.6%); mp: 247–248°C; FT-IR (KBr, ν_{max}/cm^{-1}): 3363 (N-H), 1688 (C=O), ^{1}H NMR (400 MHz, DMSO-d_6) (ppm): 2.68 (t, *J*=4.0 Hz, 4H); 3.15 (t, *J*=4.0 Hz, 4H); 3.33 (s, 2H); 6.90–7.20 (m, 6H); 7.41 (s, 2H); 11.22 (s, 1H); 12.04 (s, 1H). ^{13}C NMR (400 MHz, DMSO-d_6) (ppm): 48.48; 52.69; 60.82; 111.96; 117.31; 121.48; 122.73; 129.03; 133.91; 146.50; 150.20; 169.86 (C2'). HRMS (ESI): m/z calcd for $C_{19}H_{21}ClN_5O$ [M+H] 370.14346, found 370.1443.

In silico molecular docking

Compounds **4a-h** that exhibited cytotoxicity against liver and lung cancer cells were studied using molecular docking tools. The 3D structure of the derivatives was drawn using ChemDraw in "Mol" format. Since these compounds' molecular target(s) are currently unknown, potential tumor targets were obtained through a literature survey. X-ray crystal (3D) structure of eight selected target receptors [**Table 2**] was obtained from the Protein Data Bank (https://www.rcsb.org). CB-Dock, a blind docking network server (https://cao.labshare.cn/cb-dock/), was used for molecular docking. The downloaded formats of the docked structures were further processed using PyMOL Software (https://sourceforge.net/projects/pymol/), Protein-Ligand Interaction Profiler (https://plip-tool.biotec.tu-dresden.de/plip-web/plip/index), and LIGPLOT v.4.5.3 (https://www.ebi.ac.uk/thornton-srv/software/LIGPLOT/).

Cell culture

Cell lines were obtained from the Leibniz Institute-DSMZ (Germany). A549 (human adenocarcinomic alveolar basal epithelial) and HepG2 (human liver cancer) cells were cultured in Dulbecco's Modified Eagle's medium (Invitrogen, USA). Culture media was supplemented with fetal bovine serum (10%) (Gibco, USA).

Cell viability experiments

To assess cell growth, the MTT (3-(4,5-dimethylthiazolyl-2)-2, 5-diphenyltetrazolium bromide) cytotoxicity proliferation assay from Thermo (USA) was used. Cells were plated using 24-well NEST plates (China). Cells were then incubated with benzimidazole-piperazine derivatives using a concentration series (25, 12.5, 6.25, 2.5, and 1.25 µg/mL) for 48 h at 37°C. For evaluation of half-maximal inhibitory (IC_{50}) concentration values, MTT solution (100 µL of 5 mg/mL) was added to the growth media. Following 2 h incubation (37°C), the absorbance of the developed formazan was dissolved in DMSO and measured at 570 nm through a ChroMate plate reader (England). All results were normalized using cells treated with 1% DMSO in a complete growth medium representing 100% survival. The IC_{50} was calculated using OrignPro 8.5 software.

Table 2: PDB ID of receptors used to predict the potential anticancer activity

S. No.	PDB ID	Protein
1.	4FA6	Phosphoinositide 3-kinases alpha (PI3Ka)
2.	5EKN	Mitogen-activated protein kinase 13 (MAPK 13)
3.	1M17	Epidermal growth factor receptor (EGFR)
4.	6OQO	Cyclin-dependent kinase 4 (CDK4)
5.	4ASD	Vascular endothelial growth factor receptor 2 (VEGFR2)
6.	4UMT	Maternal embryonic leucine zipper kinase (MELK)
7.	4NUD	Bromodomain-containing protein 4 (BRD 4)
8.	1XO2	Human cyclin-dependent kinase 6 (CDK-6)

DAPI staining

The nuclear morphology changes of HepG2 cells post 48 h treatment with **4b** and **4g** were assessed by DAPI staining assay using a 24-well plate as reported in the cytotoxicity assay section. Control groups were treated with 1% DMSO, whereas, in the treatment group, **4b** and **4g** (2 × IC_{50}) were added. Post 48 h treatment, wells were rinsed with phosphate-buffered saline and then with ice-cold methanol. After that, DAPI (1 µg/mL) was used to stain the cells in the dark for 10 min, and the DNA staining was assessed using a fluorescent microscope (EVOS, USA).

AO/EB staining

HepG2 cells were treated as reported in the previous section and stained with AO/EB dual staining following the previously described method.[29] Cells were imaged using a fluorescence microscope.

CONCLUSION

This study synthesized eight benzimidazole-piperazine compounds. Testing them against lung (A549) and liver (HepG2) cancer cells revealed promising cytotoxic potential in compounds **4b, 4c, 4g**, and **4h**, possibly through apoptosis. Molecular docking identified VEGFR-2 as a potential target for these compounds.

COMPETING OF INTEREST

The authors declare no competing financial interest.

ACKNOWLEDGMENTS

The authors of this study extend their appreciation to Researchers Supporting Project (RSPD2024R757), King Saud University, Riyadh, Saudi Arabia.

REFERENCES

[1] Fei, F. and Zhou, Z. New substituted benzimidazole derivatives: A patent review (2010–2012), *Expert. Opin. Ther. Pat*., **2013**, *23*, 1157–1179.

[2] Keri, R.S., Hiremathad, A., Budagumpi, S. and Nagaraja, B.M. Comprehensive review in current developments of benzimidazole-based medicinal chemistry, *Chem. Biol. Drug. Des*., **2015**, *86*, 19–65.

[3] Tahlan, S., Kumar, S. and Narasimhan, B. Pharmacological significance of heterocyclic 1H-benzimidazole scaffolds: A review, *BMC Chem*., **2019**, *13*, 101.

[4] Pathare, B. and Bansode, T. Biological active benzimidazole derivatives, *Results Chem*., **2021**, *3*, 100200.

[5] Alam, M.M. An efficient greener strategy toward chemoselective synthesis of 1, 2-disubstituted benzimidazoles catalyzed by citric acid, *Indian J. Heterocycl. Chem*., **2022**, *32*, 15–21.

[6] Piñeros, M., Mery, L., Soerjomataram, I., Bray, F. and Steliarova-Foucher, E. Scaling up the surveillance of childhood cancer: A global roadmap, *J. Natl. Cancer Inst*., **2021**, *113*, 9–15.

[7] Cancer Therapy Advisor. (2022, February 17). *Treatment Approaches for Advanced Hepatocellular Carcinoma: Insight From the 2022 Gastrointestinal Cancers Symposium - Cancer Therapy Advisor*. https://www.cancertherapyadvisor.com/meetinginsights/muhammad-shaalan-beg-interview-hepatocellular-hcc-cancer-treatment/.

[8] Satija, G., Sharma, B., Madan, A., Iqubal, A., Shaquiquzzaman, M., Akhter, M., Parvez, S., Khan, M. and Alam, M. Benzimidazole based derivatives as anticancer agents: Structure activity relationship analysis for various targets, *J. Heterocycl. Chem*., **2022**, *59*, 22–66.

[9] Onnis, V., Demurtas, M., Deplano, A., Balboni, G., Baldisserotto, A., Manfredini, S., Pacifico, S., Liekens, S. and Balzarini, J. Design, synthesis and evaluation of antiproliferative activity of new benzimidazolehydrazones, *Molecules*, **2016**, *21*, 579.

[10] Acar Çevik, U., Sağlık, B., Korkut, B., Özkay, Y. and Ilgın, S. Antiproliferative, cytotoxic, and apoptotic effects of new benzimidazole derivatives bearing hydrazone moiety, *J. Heterocyclic. Chem*., **2018**, *55*, 138–148.

[11] Siddig, L., Khasawneh, M., Samadi, A., Saadeh, H., Abutaha, N. and Wadaan, M. Synthesis of novel thiourea-/urea-benzimidazole derivatives as anticancer agents, *Open Chem*., **2021**, *19*, 1062–1073.

[12] Xiang, Y., Chang, Y.N., Ge, Y., Kang, J.S., Zhang, Y.L., Liu, X.L., Oelschlaeger, P. and Yang, K.W. Azolylthioacetamides as a potent scaffold for the development of metallo-β-lactamase inhibitors, *Bioorg. Med. Chem. Lett*., **2017**, *27*, 5225–5229.

[13] Kurczab, R., Kucwaj-Brysz, K. and Śliwa, P. The significance of halogen bonding in ligand–receptor interactions: The lesson learned from molecular dynamic simulations of the D4 receptor, *Molecules*, **2019**, *25*, 91.

[14] Fu, Y., Zhao, J. and Chen, Z. Insights into the molecular mechanisms of protein-ligand interactions by molecular docking and molecular dynamics simulation: A case of oligopeptide binding protein, *Comput. Math. Methods Med*., **2018**, *2018*, 3502514.

[15] Xie, N.Z., Du, Q.S., Li, J.X. and Huang, R.B. Exploring strong interactions in proteins with quantum chemistry and examples of their applications in drug design, *PLoS One*, **2015**, *10*, e0137113.

[16] Hotchkiss, R.S., Strasser, A., McDunn, J.E. and Swanson, P.E. Cell death, *N. Engl. J. Med*., **2009**, *361*, 1570–1583.

[17] Chwieralski, C.E., Welte, T. and Bühling, F. Cathepsin-regulated apoptosis, *Apoptosis*, **2006**, *11*, 143–149.

[18] Elmore, S. Apoptosis: A review of programmed cell death, *Toxicol. Pathol*., **2007**, *35*, 495–516.

[19] Woo, H.Y. and Heo, J. Sorafenib in liver cancer, *Expert. Opin. Pharmacother*., **2012**, *13*, 1059–1067.

[20] Zeidan, M.A., Mostafa, A.S., Gomaa, R.M., Abou-Zeid, L.A., El-Mesery, M., A-A El-Sayed, M. and Selim, K.B. Design, synthesis and docking study of novel picolinamide derivatives as anticancer agents and VEGFR-2 inhibitors, *Eur. J. Med. Chem.*, **2019**, *168*, 315–329.

[21] Xie, Q.Q., Xie, H.Z., Ren, J.X., Li, L.L. and Yang, S.Y. Pharmacophore modeling studies of type I and type II kinase inhibitors of Tie2, *J. Mol. Graph. Model*., **2009**, *27*, 751–758.

[22] Abdullaziz, M.A., Abdel-Mohsen, H.T., El Kerdawy, A.M., Ragab, F.A.F., Ali, M.M., Abu-Bakr, S.M. Girgis, A.S. and El Diwani, H.I. Design, synthesis, molecular docking and cytotoxic evaluation of novel 2-furybenzimidazoles as VEGFR-2 inhibitors, *Eur. J. Med. Chem.*, **2017**, *136*, 315–329.

[23] Hassan, A., Badr, M., Hassan, H.A., Abdelhamid, D. and Abuo-Rahma, G.E.A. Novel 4-(piperazin-1-yl) quinolin-2 (1H)-one bearing thiazoles with antiproliferative activity through VEGFR-2-TK inhibition, *Bioorgan. Med. Chem*., **2021**, *40*, 116168.

[24] Machado, V.A., Peixoto, D., Costa, R., Froufe, H.J.C., Calhelha, R.C., Abreu, R.M.V., Ferreira, I.C.F.R., Soares, R. and Queiroz, M.J.R.P. Synthesis, antiangiogenesis evaluation and molecular docking studies of 1-aryl-3-[(thieno [3, 2-b] pyridin-7-ylthio) phenyl] ureas: Discovery of a new substitution pattern for type II VEGFR-2 Tyr kinase inhibitors, *Bioorgan. Med. Chem*., **2015**, *23*, 6497–6509.

[25] Sobhy, M.K., Mowafy, S., Lasheen, D.S., Farag, N.A. and Abouzid, K.A.M. 3D-QSAR pharmacophore modelling, virtual screening and docking studies for lead discovery of a novel scaffold for VEGFR 2 inhibitors: Design, synthesis and biological evaluation, *Bioorg. Chem*., **2019**, *89*, 102988.

[26] Wang, Z., Wang, N., Liu, P., Chen, Q., Situ, H., Xie, T., Zhang, J., Peng, C., Lin, Y. and Chen, J. MicroRNA-25 regulates chemoresistance-associated autophagy in breast cancer cells, a process modulated by the natural autophagy inducer isoliquiritigenin, *Oncotarget*, **2014**, *5*, 7013–7026.

[27] Shahin, M.I., Abou El Ella, D.A., Ismail, N.S.M. and Abouzid, K.A.M. Design, synthesis and biological evaluation of type-II VEGFR-2 inhibitors based on quinoxaline scaffold, *Bioorg. Chem*., **2014**, *56*, 16–26.

[28] Abbhi, V., Saini, L., Mishra, S., Sethi, G., Kumar, A.P. and Piplani, P. Design and synthesis of benzimidazole-based Rho kinase inhibitors for the treatment of glaucoma, *Bioorg. Med. Chem*., **2017**, *25*, 6071–6085.

[29] Abutaha, N., AL-Mekhlafi, F., Almutairi, B. and Wadaan, M. S-phase cell cycle arrest, and apoptotic potential of Echium arabicum phenolic fraction in hepatocellular carcinoma HepG2 cells, *J. King Saud Univ. Sci*., **2022**, *34*, 101735.

Received: 06 Aug 2023; Accepted: 11 Dec 2023